applied sciences

MDPI

Article

Numerical Investigation into the Mechanical Behaviours and Energy Characteristics of Hard Coal Subjected to Coupled Static-Dynamic Loads

Jiachuan Sun [1,2], Linming Dou [1], Guifeng Wang [1], Lihai Tan [1,3,4,*] and Huaide Peng [4]

[1] School of Mines, China University of Mining and Technology, Xuzhou 221116, China
[2] Junde Coal Mine, Longmei Mining Co., Ltd., Hegang 154100, China
[3] School of Civil, Mining and Environmental Engineering, University of Wollongong, Wollongong, NSW 2522, Australia
[4] School of Resource Environment and Safety Engineering, University of South China, Hengyang 412001, China
* Correspondence: lt716@uowmail.edu.au

Abstract: In practical engineering, coal burst is usually caused by the combination of high geo-stress and dynamic loading. To study the dynamic response of coal in geo-stress conditions, numerical models of a coupled static–dynamic split Hopkinson pressure bar (SHPB) test system were established, based on which impact tests for coal specimens at different impact speeds and static pre-stress levels were conducted. The mechanical properties, energy characteristics and failure patterns of coal specimens under coupled static and dynamic loads were analyzed. The results show that when the pre-stress is constant, peak stress, the maximum strain energy and the maximum kinetic energy increase significantly with impact speed. Nevertheless, they are less affected by the static pre-stress, increasing linearly with a pre-stress level under lower impact speeds but becoming stable under higher impact speeds. In addition, weak dynamic loads may trigger the instability of the coal specimen in a high pre-stress condition. Overall, both the impact speed and static pre-stress have influence on the mechanical behavior and energy characteristics of coal specimens under coupled static and dynamic loads, but the influence of the impact speed outweighs that of the static pre-stress.

Keywords: numerical modeling; coupled static and dynamic loads; coal burst; energy evolution

Citation: Sun, J.; Dou, L.; Wang, G.; Tan, L.; Peng, H. Numerical Investigation into the Mechanical Behaviours and Energy Characteristics of Hard Coal Subjected to Coupled Static-Dynamic Loads. *Appl. Sci.* **2023**, *13*, 892. https://doi.org/10.3390/app13020892

Academic Editors: Rihong Cao, Shijie Xie and Hang Lin

Received: 20 December 2022
Revised: 6 January 2023
Accepted: 6 January 2023
Published: 9 January 2023

1. Introduction

In deep underground coal mines, the strata and coal seams are always subjected to both static geo-stress and dynamic stress disturbance. Therefore, coal burst hazards usually result from the superposition of dynamic and static loads [1,2]. The quasi-static and dynamic mechanical behaviors of rock mass and coal have been investigated in a large number of theoretical and experimental studies [3,4]. It is well known that the mechanical behaviors of rock mass and coal under dynamic loading conditions are quite different from those under quasi-static conditions due to the strain rate effect. Materials with higher strain rates are more likely to show greater strength during mechanical tests, while their mechanical behaviors become more complex when the static and dynamic loading are both considered. The burst threshold and energy evolution of the coal body may vary from case to case, because it depends on the couple static and dynamic loading conditions. Therefore, the coupled effect of static and dynamic loads is expected to be considered in practical engineering, especially for dynamic disasters.

As an ideal and reliable mechanical test apparatus to study the dynamical mechanical behaviors of rock, the split Hopkinson pressure bar (SHPB) system has been widely used to determine the dynamic response and instability characteristics of rock mass and coal under high strain rates [5–8]. To study the mechanical behaviors of rock mass under coupled static–dynamic loads, Li et al. [9] developed an improved SHPB system which

allows the specimen to be subjected to coupled axial static pre-stress and axial impact loading. Based on the coupled static–dynamic SHPB test method, great progress has been made in terms of the study of the mechanical behaviors of rock mass in complex stress conditions. Li et al. [10] revealed that for a given static pre-stress, rock strength rises with the increase in dynamic loads. Moreover, the increase in pre-stress may change the failure patterns and results in more shear cracks. Tao et al. [11] conducted a series of coupled static and dynamic loading tests of rock specimen with a hole and investigated the dynamic failure characteristics of rock specimens at different pre-stress levels. The result shows that static pre-stress strongly affects the failure intensity and the primary fractures are caused by the combination of both static and dynamic stress. Peng et al. [12] experimentally investigated the mechanical behaviors of rock specimens containing two non-coplanar fissures. Cheng et al. [13] reveal that the effect of confining stress on the dynamic strength of coal may be greater than that of axial pre-stress. Their results show that the specimens' mechanical properties are highly dependent on the dynamic strain rate when the static pre-stress keeps constant in some cases.

The coupled static and dynamic mechanical behaviors of rock mass in non-coal underground mines have been extensively investigated in many studies, as mentioned above. Compared to the rock mass, coal is always characterized by lower strength and less bump proneness [14]. Nevertheless, with the increase in mining depth, coal mining may be associated with coal burst hazards as the coal body is generally highly stressed in deep coalmines. As a result, more and more coal bump hazards are happening in many coal mining countries including the USA, China, Poland and Australia [15–17]. However, studies on dynamical–mechanical response characteristics of coal under coupled static and dynamic stress conditions remain insufficient. More studies are expected to improve the understanding of the mechanical behaviors and instability mechanism of coal under coupled static and dynamic stress conditions.

Compared with laboratory experiments, numerical simulations are able to exactly record the stress and energy states and failure evolution, which is helpful in the determination of specimens' mechanical behavior and their failure mechanism. In addition, one possible problem in the experimental SHPB tests is that the precision of test results greatly depends on measuring apparatuses such as strain gauges. Due to the weakness of coal, however, the amplitude of the reflected stress wave may be very close to that of the incident stress wave, which may increase the test error. As the data can be exactly recoded without error, such problems can be completely avoided in the numerical simulations, which provide reliable results. In this study, numerical coupled static and dynamic SHPB models based on a discrete element method (DEM) were established, on the basis of which a series of impact tests were conducted for hard coal specimens with different impact speeds and static pre-stress levels. The dynamic mechanical properties, energy characteristics and failure patterns were investigated for the purpose of a comprehensive understanding of the dynamic mechanical behaviors of hard coals.

2. Methods

2.1. SHPB System

The SHPB system, originally developed by Kolsky to obtain the dynamic stress–strain relationship of several materials [18], has been taken as the most successful loading technique for investigating the dynamic characteristics of rock [19]. After more than a decade's development and modification by geotechnical researchers, SHPB system now can be used for coupled static and dynamic loading test considering axial stress and confining stress. Frew et al. [20] modified the conventional SHPB apparatus by adding a thin copper disk to the impact surface of the incident bar to obtain compressive stress–strain data for rock materials. Li et al. [9] developed a new testing system for coupling static and dynamic load experiments on rock based on a previous SHPB system. Bailly et al. [21] proposed a new technique based on an SHPB system to achieve triaxial compression loading of materials. The detailed introduction to SHPB history as well as its modification

and application have been comprehensively reviewed in literatures [22]. Furthermore, the pulse-shaping techniques and stress–strain equilibrium of SHPB tests have additionally been thoroughly studied by many researchers [23,24]. In this paper, the SHPB system was adopted to apply coupled static and dynamic loads on a coal sample in order to investigate the stress–strain relationship, failure mode and energy evolution of coal subjected to coupled static and dynamic loads.

The principle of the SHPB system for coupling static and dynamic loads experiment is briefly described in this section. As shown in Figure 1, the numerical modeling is based on the experimental coupled static and dynamic SHPB system developed by Li et al. [9]. It involves a striker bar, an incident bar and a transmission bar according to the standards proposed by the International Society for Rock Mechanics (ISRM) [25]. In addition, a pre-loading unit was mounted to apply static pre-stress before the impact test. The specimen was sandwiched between the incident and transmission bar. First, a given axial pre-stress will be applied to the specimen by the pressure loading unit at the end of the transmission bar. The strike bar will then be released to impact the incident bar once the pre-stress condition is stable within the SHPB system and specimen.

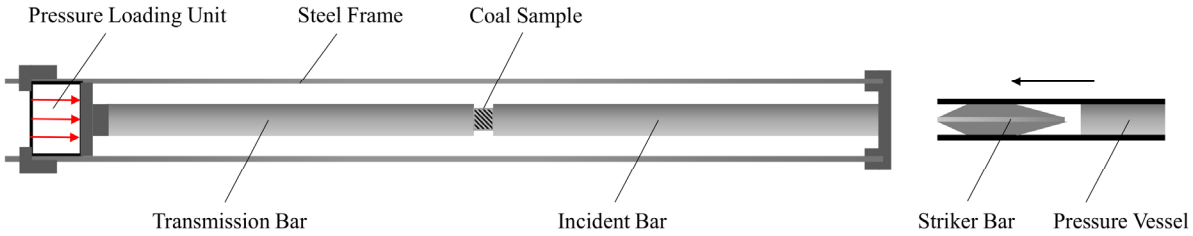

Figure 1. Schematic diagram of SHPB system for coupling loads experiment.

The strain rate $\dot{\varepsilon}(t)$, strain $\varepsilon(t)$ and stress $\sigma(t)$ of sample can be expressed according to one-dimensional stress wave theory [26]:

$$\dot{\varepsilon}(t) = -2\frac{C}{L_S}\varepsilon_R(t) \tag{1}$$

$$\varepsilon(t) = -2\frac{C}{L_S}\int_0^t \varepsilon_R(t)dt \tag{2}$$

$$\sigma(t) = \frac{EA}{A_s}\varepsilon_T(t) \tag{3}$$

where C is the elastic wave speed in the bars, L_S and A_s are the cross-sectional area and the length of the sample, and E is the Young's modulus of bars. Detailed explanation and derivation procedures of these three equations have been given by Shan et al. [27].

2.2. Extension of PFC Modeling

PFC is a widely used commercial software for many research and industrial projects developed by the ITASCA Consulting Group. The PFC uses a bonded particle model (BPM) to represent the geo-material as an assembly of stiff discs (2D) or spheres (3D) that interact at contacts and are held together by internal forces and moments. The internal forces and moments are updated using contact mechanics, and the explicit dynamic solution to Newton's equations of motion is used to compute the velocity of the particles. In this study, the failure behavior and energy evolution of the coal sample under coupled static and dynamic compression loads were simulated using the PFC in two dimensions (PFC2D), which is an effective software to successfully reproduce many features and behaviors of rock, including elasticity, cracking, damage accumulation, energy evolution, post-peak softening, and strength increase with confinement.

In the PFC^{2D}, the interaction between particles can be defined by two models, namely the contact bond model and the parallel bond model [28]. The contact point in a constant

model is given a tensile normal and shear contact-force strength that can bear a tensile force but cannot resist the moment [29]. The parallel bond model, which is more suitable for simulating rock materials because it is capable of resisting the moment [30], establishes an elastic interaction between particles that can resist against separation under tension, shear and rotation. Therefore, to establish a suitable numerical model of coal samples, the linear parallel bond proposed by Potyondy and Cundall [31] was adopted to define the connection between particles in this study.

The numerical model of the coupled static and dynamic SHPB system is presented in Figure 2.

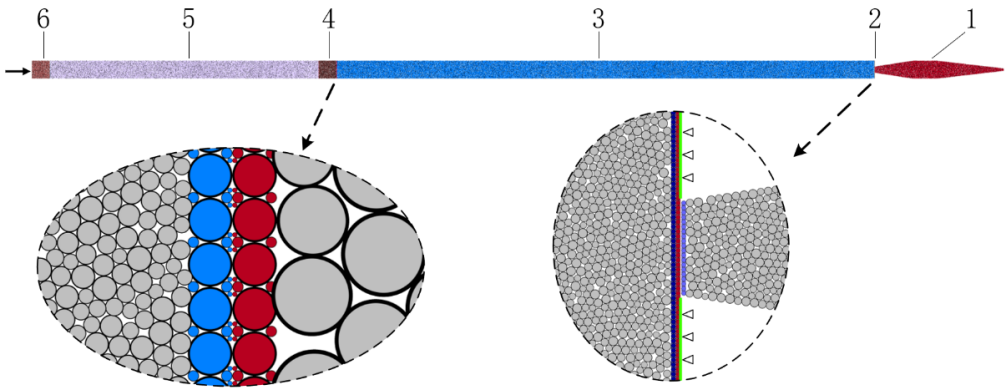

Figure 2. Numerical model of SHPB test system (1: Striker, 2: Fixed board, 3: Incident bar, 4: Specimen, 5: Transmitted bar, 6: Absorbing bar).

3. Numerical Models

3.1. Model Parameters

Standard uniaxial compression tests were conducted in the laboratory to determine the static mechanical properties of the coal specimens, based on which a series of trial-and-error numerical simulations were performed to determine the optimal parameters of the numerical specimens. Some coal blocks were taken from an underground coal mine suffering from coal bump hazards. The coal blocks were then cut into a series of cylindrical specimens with a dimension of 54 mm × 108 mm (radius × height). All the specimens were polished to make sure their conditions, including parallelism, flatness and verticality, met the standard established by the International Society of Rock Mechanics. Subsequently, standard uniaxial compression tests were conducted for the specimens using an Instron 8033 loading machine with a displacement control loading rate of 0.5 mm/min. The loading data including force and displacement were recorded by the loading system during the tests. Figure 3 presents the stress–strain curve of a typical coal specimen and its failure pattern. Table 1 presents the calibrated mesoscopic parameters of the specimens in the numerical simulations according to the laboratory results.

3.2. Loading Applying

In this study, the pre-stress coefficient k_s is defined as the ratio of the pre-stress to the static uniaxial compressive strength of the specimen. Six impact speeds are considered, namely 4 m/s, 6 m/s, 8 m/s, 10 m/s, 12 m/s and 14 m/s. For each given impact speed, the impact tests were conducted nine times at different pre-stress levels with the pre-stress coefficient k_s increasing from 0.0 to 0.8 with an interval of 0.1. When k_s is 0.0, it means that there is no pre-stress. Overall, 54 coupled static and dynamic SHPB tests with different impact speeds and pre-stress levels were carried out in the numerical simulations.

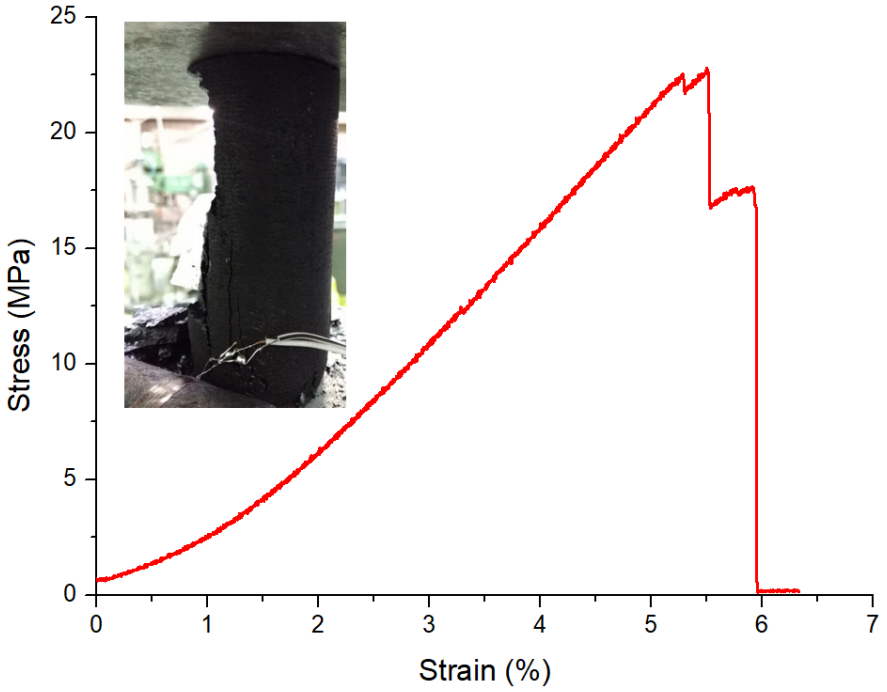

Figure 3. Experimental results of coal sample subject to uniaxial compression.

Table 1. Mesoscopic parameters of the numerical specimens.

Particle Basic Parameters		Parallel Bond Parameter	
Particle contact modules E_c (GPa)	1.8	Elasticity modulus $\overline{E_c}$(GPa)	1.8
Stiffness ratio k_n/k_s	1.0	Stiffness ratio k_n/k_s	1.0
Particle friction coefficient μ	0.577	Cohesion $\bar{c}$(MPa)	12.3
Particle density $\rho(g/cm^3)$	1.4	Tensile Strength $\overline{\sigma_c}$(MPa)	7.7

4. Numerical Simulation

4.1. Stress Characteristics

As shown in Figure 4a, there is a positive approximate linear relation between impact speed and peak stress in all cases with different pre-stress levels. For specimens under the same impact speed with different pre-stress levels, though the peak stress varies to some extent, the slopes of their impact speed and peak stress curves are very similar to each other. With the impact speed increasing from 4 m/s to 14 m/s, the peak stress increases from 25.2 MPa to 53.2 MPa when k_s is 0 and from 35.6 MPa to 60.1 MPa when it is 0.8, respectively. Overall, the influence of the impact speed on the dynamic strength of coal specimens is very significant in spite of varying pre-stress levels.

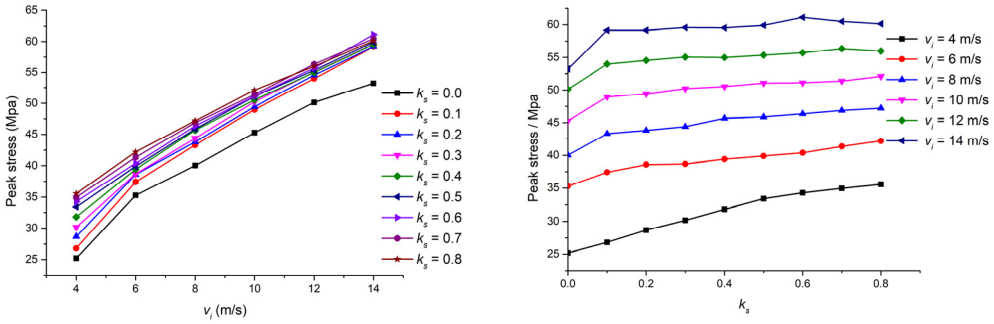

(**a**) The curves of v_i vs. peak stress (**b**) The curves of k_s vs. peak stress

Figure 4. Peak stress of coal specimens subjected to different pre-stress levels and impact speeds.

Compared to impact speed, pre-stress has less influence on the dynamic strength of the coal specimens. As shown in Figure 4b, under the lower impact speed of 4 m/s, the peak stress increases linearly from 25.1 MPa to 35.6 MPa with k_s increasing from 0 to 0.8. With the increase in impact speed, the relation between the pre-stress coefficient and peak stress gradually becomes non-linear while the growth rate of the peak stress with the increase in the pre-stress coefficient also decreases. When the impact speed reaches 14 m/s, the peak stress increases from 53.2 MPa to 59.1 MPa by 11.0% when k_s increase from 0.0 to 0.1 and remains stable when the pre-stress coefficient further increases to 0.8. In such a case, the influence of the pre-stress is not obvious anymore.

4.2. Energy Characteristics

To investigate the energy characteristics of the coal specimens, the strain energy and kinetic energy were recorded during the impact tests. In the DEM numerical models, the strain energy of the specimen refers to the sum of the strain energy stored in all contacts in the specimen and the kinetic energy refers to the sum of the kinetic energy of all particles in the specimen. In this study, energy density is defined as the energy in the specimen per unit volume. Figure 5 presents the curves of strain energy density vs. k_s for coal specimens at three typical impact speeds. Figure 6 further gives the maximum strain energy per unit volume in coal specimens subjected to different pre-stress levels and impact speeds. It can be seen that the impact speed has a remarkable influence on the strain energy release characteristics. When the impact speed is only 4 m/s, the strain energy release is relatively slow. At the end of the impact test (impact time = 600 us), all specimens have residual strain energy inside them. For specimens under the impact speed of 8 m/s, the strain release rate is much higher than that under the impact speed of 4 m/s. Furthermore, at the end of the impact test, the residual strain energy is also much lower. For specimens at high pre-stress levels ($k_s \geq 0.7$), the residual strain energy is close to zero, which means that the broken specimens in such cases lose almost their whole energy storage capacity. When the impact speed reaches 14 m/s, the strain energy drops sharply after the peak point in all cases, indicating that specimens are suffering violent energy release, which may cause serious failure and fragment ejection. Moreover, there is no residual strain energy of all specimens under such a high impact speed; namely, these specimens are all completely broken.

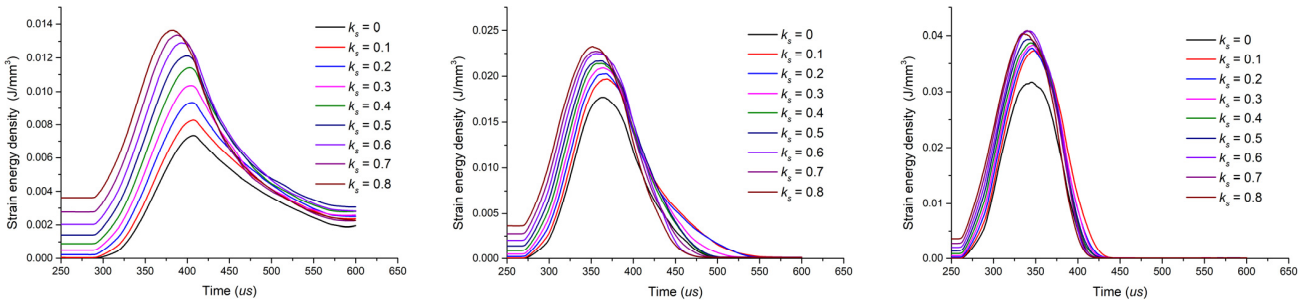

(**a**) v_i = 4 m/s (**b**) v_i = 8 m/s (**c**) v_i = 14 m/s

Figure 5. The curves of strain energy per unit volume vs. k_s for coal specimens subjected to different pre-stress levels and impact speeds.

Generally, the strain energy release characteristics directly associate with the impact speed; a higher impact speed contributes to more strain energy stored in the specimen and a faster energy release rate during the instability stage of the specimen. Compared with the impact speed, pre-stress has less influence on the strain energy. For the specimen under a low impact speed of 4 m/s, the strain energy release rate rises gradually with the increase in the pre-stress coefficient (Figure 5a). However, when the impact speed increases to 8 m/s or 14 m/s, the influence of the pre-stress coefficient on strain energy release is not clear anymore. For specimens at a lower impact speed, the relation between pre-stress

and the strain energy per unit volume is approximately linear, but this relation gradually becomes unclear with the increase in the impact speed.

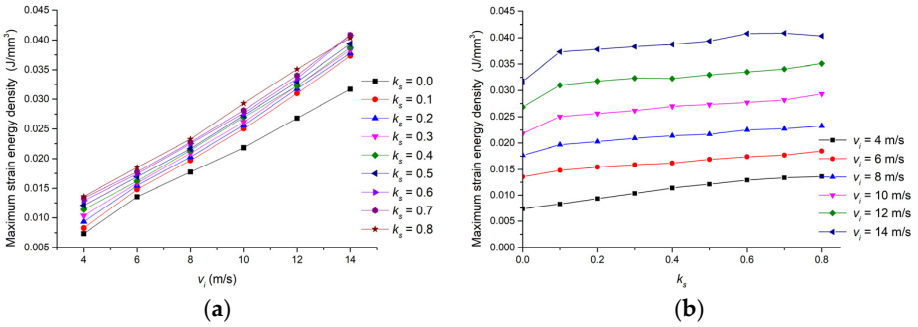

(**a**) (**b**)

Figure 6. The maximum strain energy per unit volume within coal specimens subjected to different pre-stress levels and impact speeds. (**a**) The curves of v_i vs. maximum strain energy per unit volume; (**b**) The curves of k_s vs. maximum strain energy per unit volume.

When a coal burst happens, it is always characterized by violent fragment ejection with high kinetic energy. Therefore, it is of great importance to determine the kinetic energy response characteristics of the coupled static and dynamic loads. Figure 7 presents the maximum kinetic energy per unit volume of coal specimens subjected to different pre-stress levels and impact speeds during impact tests. It can be seen from Figure 7a that with the increase in the impact speed, the maximum kinetic energy per unit volume first increases slowly and then begins to increase rapidly when the impact speed exceeds about 6 m/s. As shown in Figure 7b, however, for a given impact speed, the value of the maximum kinetic energy per unit volume fluctuates without a clear law when the pre-stress coefficient increases from 0.0 to 0.8.

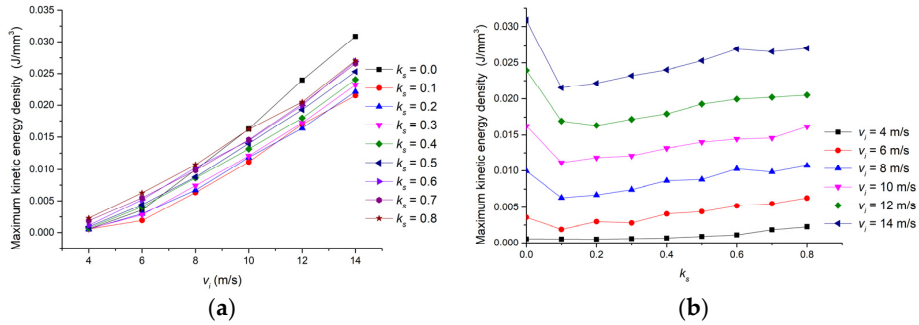

(**a**) (**b**)

Figure 7. The maximum kinetic energy per unit volume of coal specimens subjected to different pre-stress levels and impact speeds. (**a**) The curves of v_i vs. maximum kinetic energy per unit volume; (**b**) The curves of k_s vs. maximum kinetic energy per unit volume.

4.3. Failure Patterns

Figure 8 presents the failure patterns of specimens at different impact speeds without pre-stress. The failure patterns of coal specimens with different pre-stress levels at three typical impact speeds, namely 4 m/s, 8 m/s and 14 m/s, are shown in Figures 9–11, respectively. When there is no pre-stress, the specimen remains intact with only a few small cracks scattered within it at the impact speed of 4 m/s. Subsequently, with the increase in the impact speed, the failure of the specimens gradually becomes serious, with an increasing number of cracks and fragments (Figure 8). It can be seen from Figure 10 that for specimens at the low impact speed (4 m/s), the specimen remains intact with a pre-stress coefficient of 0.1 after the impact test (Figure 10a). When the pre-stress coefficient increases to 0.2, the specimen is slightly broken by two cracks close to the upper and lower sides. Subsequently, with the increase in the pre-stress coefficient, the failure pattern becomes more serious with increasing cracks and fragments. However, when the specimens

are tested under higher impact speeds, the pre-stress level shows little influence on the fracture pattern of specimens, as shown in Figures 10 and 11. Though the failure intensity of specimens clearly increases with the increase in the impact speed from 4 m/s to 14 m/s, it fails to experience significant change with the increasing pre-stress level when the impact speed is no less than 8m/s. It can be concluded that the influence of the impact speed on failure patterns is greater than that of the pre-stress. For specimens under lower impact speeds, pre-stress helps trigger specimen instability and increases its failure intensity. For those at higher impact speeds, however, the mechanical behavior of specimens is mainly controlled by the higher impact speed while the influence of the pre-stress is quite limited.

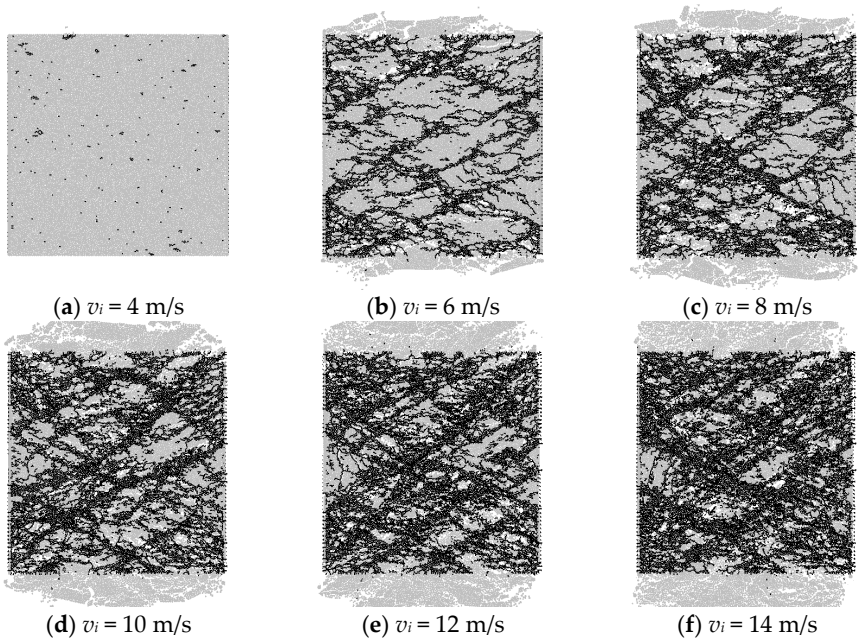

(**a**) v_i = 4 m/s (**b**) v_i = 6 m/s (**c**) v_i = 8 m/s

(**d**) v_i = 10 m/s (**e**) v_i = 12 m/s (**f**) v_i = 14 m/s

Figure 8. Failure patterns of specimens at different impact speeds without pre-stress.

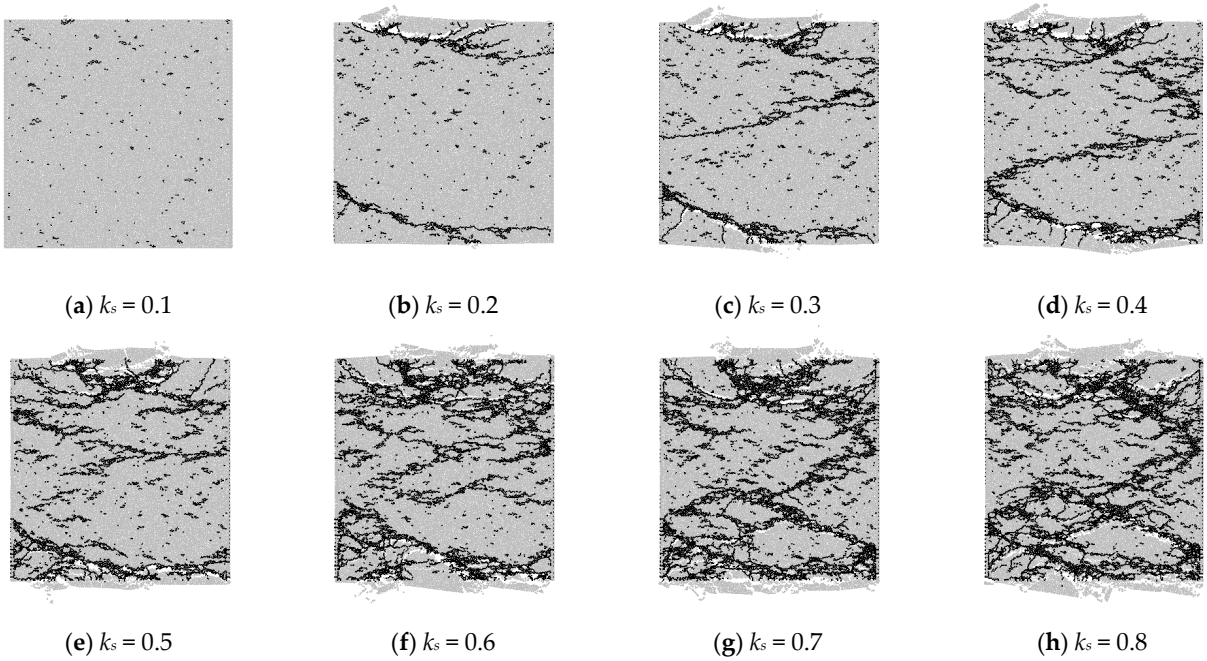

(**a**) k_s = 0.1 (**b**) k_s = 0.2 (**c**) k_s = 0.3 (**d**) k_s = 0.4

(**e**) k_s = 0.5 (**f**) k_s = 0.6 (**g**) k_s = 0.7 (**h**) k_s = 0.8

Figure 9. Failure mode of sample subject to different pre-stress levels at 4 m/s impact speed.

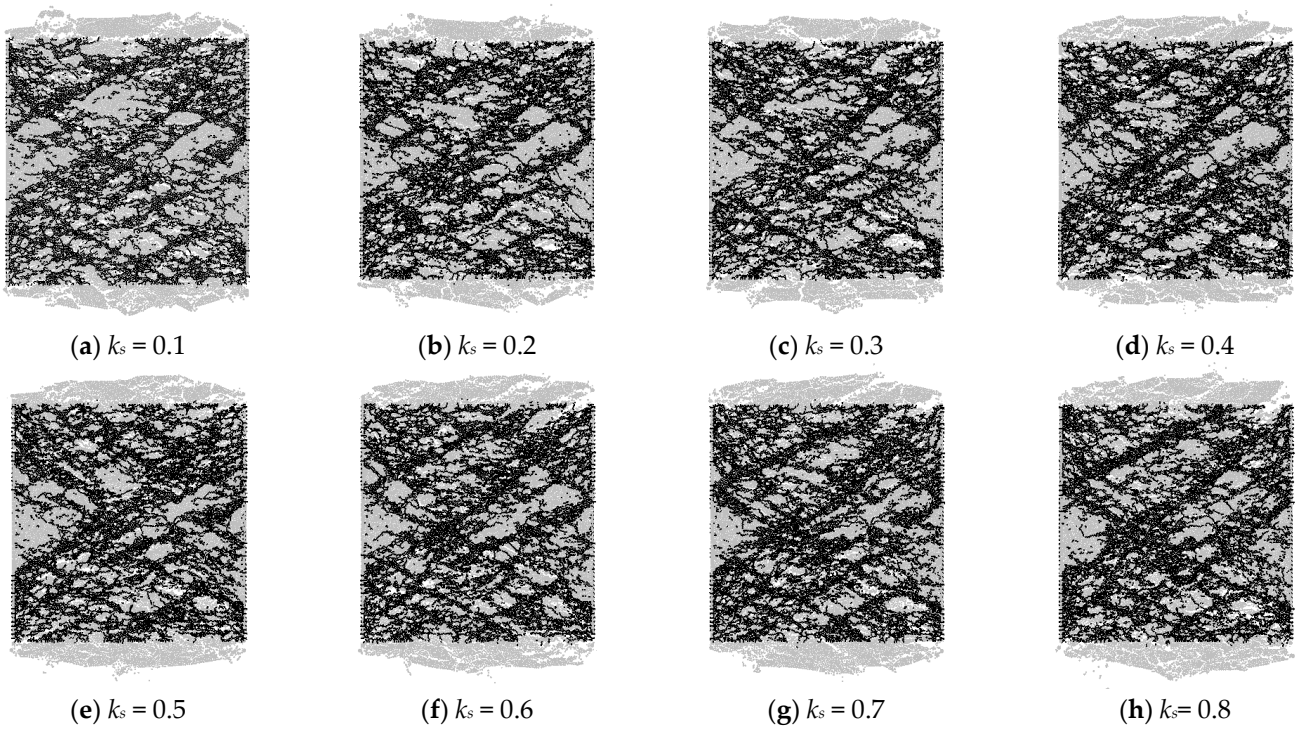

(**a**) k_s = 0.1 (**b**) k_s = 0.2 (**c**) k_s = 0.3 (**d**) k_s = 0.4

(**e**) k_s = 0.5 (**f**) k_s = 0.6 (**g**) k_s = 0.7 (**h**) k_s= 0.8

Figure 10. Failure mode of sample subject to different pre-stress levels at 8 m/s impact speed.

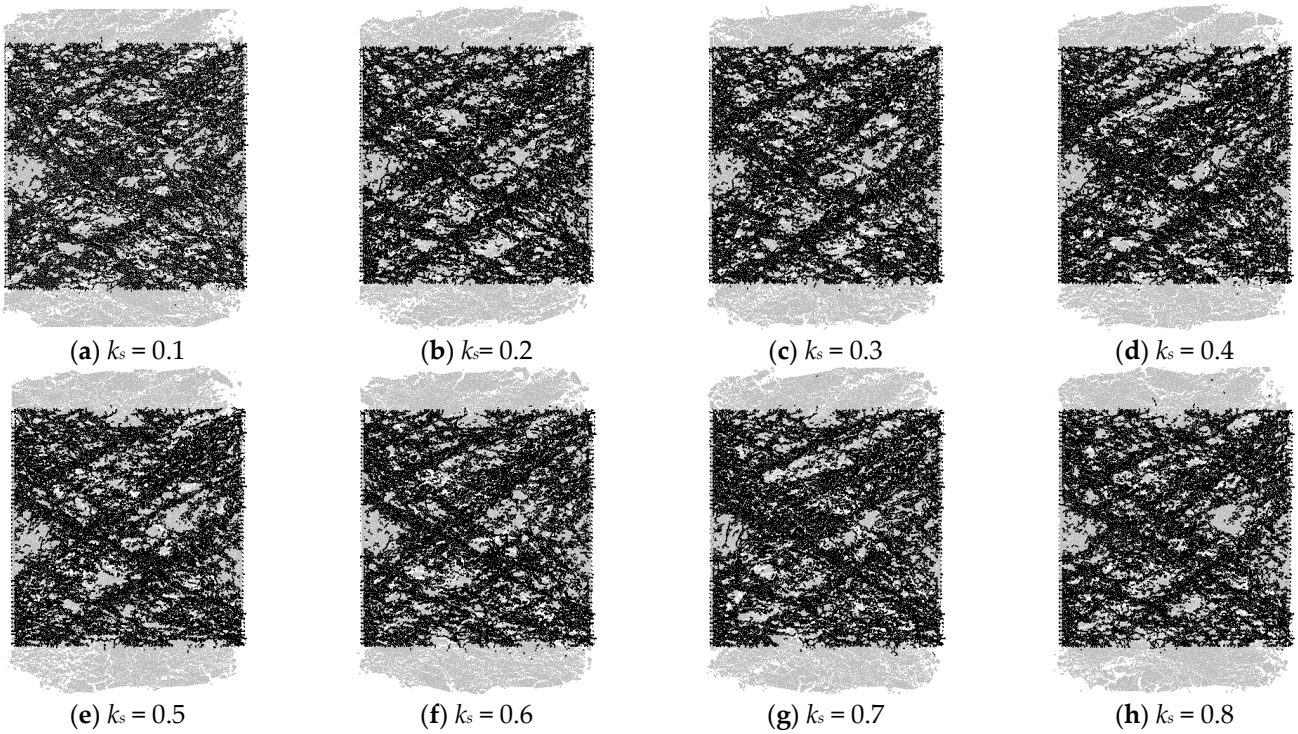

(**a**) k_s = 0.1 (**b**) k_s= 0.2 (**c**) k_s = 0.3 (**d**) k_s = 0.4

(**e**) k_s = 0.5 (**f**) k_s = 0.6 (**g**) k_s = 0.7 (**h**) k_s = 0.8

Figure 11. Failure mode of sample subject to different pre-stress levels at 14 m/s impact speed.

5. Discussion

Based on DEM numerical simulations, this study investigated the stress characteristics, energy characteristics and failure patterns of coal specimens under coupled static and dynamic loads; similar results for rock specimens have been obtained in earlier experimental studies [10,12], which confirm the validity of this numerical study. It is generally agreed that the strengthening mechanism of specimens' mechanical properties under coupled

static and dynamic loads is that the static pre-stress promotes the original micro-cracks close within the specimens, increasing their wave impedance and thus improving their dynamic strength [32,33]. In this study, however, the original micro-cracks were not taken into consideration in the numerical modelling, but the test results concluded from the numerical simulations are similar to those from experiments in the above-mentioned studies. Therefore, we suppose that the increase in the specimens' strength under coupled static and dynamic loading conditions is partly attributed to the superposition of the static pre-stress and the dynamic stress wave.

In this study, the results show that the relation between coal dynamic strength and the pre-stress coefficient is positive. The dynamic strength increases with the pre-stress coefficient increasing from 0 to 0.8. However, some experimental results show that for natural rock mass, with the increase in pre-stress levels, the dynamic strength increases first and then decreases. The rock specimens have a maximum dynamic compressive strength at the axial compression ratio of about 0.6–0.7 [10,12,34]. This difference between the numerical and experimental results may be caused by the anisotropy and micro-flaws within the natural rock mass. For the rock mass, local failure may appear due to natural micro-flaws in weak areas under pre-stress conditions. Once the axial pre-stress reaches a certain level, it may give rise to obvious plastic deformation within the specimen before the impact test and thus decrease the dynamic mechanical properties of the specimens. In addition, natural micro-flaws and those produced by the pre-stress contribute to the reflection of the tensive stress waves during impact and the propagation of cracks. However, in the numerical study, the natural micro-flaws and anisotropy within the specimens were not considered. As a result, little failure appeared within the elastic-deformed specimens even at a high pre-stress level. Accordingly, the pre-stress failed to show its negative effect on the mechanical properties in the numerical simulations. Constitutive models considering the initial void compaction or original failure within the specimens may help address this problem and be better at describing the realistic mechanical behavior of natural rock mass and coal in numerical simulations [35–37], which are expected in future studies. Comparing this numerical study with earlier experimental studies shows that pre-stress contributes to the increase in specimens' dynamic strength during the elastic deformation stage while this effect turns out to be negative when the pre-stress exceeds its elastic limit.

6. Conclusions

In this study, a coupled static and dynamic SHPB apparatus was replicated using the DEM numerical method. The main conclusions are listed as follows:

(1) The influence of dynamic loading on both stress and energy characteristics is remarkable with clear laws. When the pre-stress is constant, with the increase in the impact speed within the research range, both dynamic strength and maximum strain energy of the specimen increase in an approximately linear way. The maximum kinetic energy grows slowly at first and then grows rapidly. The dynamic loading also strongly affects the release characteristics of the strain energy. Higher impact speeds contribute to more strain energy stored with the specimen and more violent release of it.

(2) A static pre-stress only shows a clear influence on the strain energy characteristics when the dynamic loading is weak; namely, when the impact speed is relatively low. In such a case, the value of the maximum strain energy stored in the specimen increases slowly in an approximate way with the increase in the pre-stress. However, with the increase in the impact speed, the influence of the pre-stress on the strain energy characteristics decreases with a less clear change law. As for the maximum kinetic energy stored in the specimen during the impact test, the pre-stress fails to show a remarkable and clear influence on it.

(3) Pre-stress affects the mechanical behavior of specimens significantly at lower impact speeds. Even if a low-speed impact fails to break the specimens without pre-stress or at lower pre-stress levels, it may be able to trigger the instability of the specimen at higher pre-stress levels. However, for specimens at higher impact speeds which are

enough to break them without pre-stress, pre-stress has limited influence on the peak stress of the specimens, but hardly affects their failure pattern, which is dominated by the high impact speed.

Author Contributions: Conceptualization, J.S. and L.T.; methodology, L.D.; software, L.T.; validation, G.W.; formal analysis, G.W.; investigation, J.S.; resources, L.D.; data curation, J.S.; writing—original draft preparation, J.S.; writing—review and editing, L.T. and H.P.; visualization, L.T. and H.P.; supervision, L.D.; project administration, L.D.; funding acquisition, L.D. All authors have read and agreed to the published version of the manuscript.

Funding: This research was funded by the National Natural Science Foundation of China, grant number 51934007, the Department of Education of Hunan Province, grant number 19B479, and the Natural Science Foundation of Hunan Province, grant number 2022JJ40351.

Institutional Review Board Statement: Not applicable.

Informed Consent Statement: Not applicable.

Data Availability Statement: Data are available from the corresponding author upon reasonable request.

Conflicts of Interest: The authors declare no conflict of interest.

References

1. Yang, X.H.; Ren, T.; Alex, R.; He, X.Q.; Tan, L.H. Analysis of Energy Accumulation and Dissipation of Coal Bursts. *Energies* **2018**, *11*, 1816. [CrossRef]
2. Zhong, K.; Zhao, W.; Qin, C.; Gao, H.; Chen, W. Mechanical Properties of Roof Rocks under Superimposed Static and Dynamic Loads with Medium Strain Rates in Coal Mines. *Appl. Sci.* **2021**, *11*, 8973. [CrossRef]
3. Tan, L.; Ren, T.; Dou, L.; Yang, X.; Qiao, M.; Peng, H. Analytical stress solution and mechanical properties for rock mass containing a hole with complex shape. *Theor. Appl. Fract. Mech.* **2021**, *114*, 103002. [CrossRef]
4. Tan, L.; Ren, T.; Dou, L.; Yang, X.; Cai, X.; Qiao, M. Analytical stress solution for rock mass containing two holes based on an improved Schwarz alternating method. *Theor. Appl. Fract. Mech.* **2021**, *116*, 103092. [CrossRef]
5. Tan, L.; Zhou, Z.; Cai, X.; Rui, Y. Analysis of mechanical behaviour and fracture interaction of multi-hole rock mass with DIC measurement. *Measurement* **2022**, *191*, 110794. [CrossRef]
6. Wang, Y.; Yang, Y.; Zhang, Y.; Wang, J. Dynamic Mechanical Properties of Coals Subject to the Low Temperature-Impact Load Coupling Effect. *Sci. Rep.* **2019**, *9*, 20218. [CrossRef]
7. Tao, M.; Zhao, H.; Momeni, A.; Cao, W.; Zhao, Y. Dynamic failure behavior and damage evolution process of holed sandstone under impact loads. *Int. J. Damage Mech.* **2022**, *32*, 28–49. [CrossRef]
8. Zhao, H.; Tao, M.; Li, X.; Hong, Z.; Zhao, R.; Cao, W. Experimental investigation on dynamic mechanical properties and fracture evolution behavior of the underground openings with excavation damaged zones. *Int. J. Damage Mech.* **2022**, *31*, 1533–1561. [CrossRef]
9. Li, X.; Zhou, Z.; Lok, T.-S.; Hong, L.; Yin, T. Innovative testing technique of rock subjected to coupled static and dynamic loads. *Int. J. Rock Mech. Min. Sci.* **2008**, *45*, 739–748. [CrossRef]
10. Li, X.; Zhou, Z.; Zhao, F.; Zuo, Y.; Ma, C.; Ye, Z.; Hong, L. Mechanical properties of rock under coupled static-dynamic loads. *J. Rock Mech. Geotech. Eng.* **2009**, *1*, 41–47. [CrossRef]
11. Tao, M.; Ma, A.; Cao, W.; Li, X.; Gong, F. Dynamic response of pre-stressed rock with a circular cavity subject to transient loading. *Int. J. Rock Mech. Min. Sci.* **2017**, *99*, 1–8. [CrossRef]
12. Feng, P.; Dai, F.; Liu, Y.; Du, H.-B. Mechanical behaviors of rock-like specimens with two non-coplanar fissures subjected to coupled static-dynamic loads. *Eng. Fract. Mech.* **2018**, *199*, 692–704. [CrossRef]
13. Cheng, C.; Xue, S.; Han, Y. Experimental Study on the Mechanical Behavior of Coal under Triaxial Dynamic Compression. *Minerals* **2022**, *12*, 1206. [CrossRef]
14. Lin, B.; Zou, Q.; Liang, Y.; Xie, J.; Yang, H. Response characteristics of coal subjected to coupling static and waterjet impact loads. *Int. J. Rock Mech. Min. Sci.* **2018**, *103*, 155–167. [CrossRef]
15. Justine, C.; Jan, N. Coalburst Causes and Mechanisms. Proceedings of Coal Operators Conference, Wollongong, NSW, Australia, 10–12 February 2016.
16. Mark, C. Coal bursts that occur during development: A rock mechanics enigma. *Int. J. Min. Sci. Technol.* **2018**, *28*, 35–42. [CrossRef]
17. Yang, X.H.; Ren, T.; Tan, L.H.; Remennikov, A.; He, X.Q. Developing coal burst propensity index method for Australian coal mines. *Int. J. Min. Sci. Technol.* **2018**, *28*, 783–790. [CrossRef]
18. Demirdag, S.; Tufekci, K.; Kayacan, R.; Yavuz, H.; Altindag, R. Dynamic mechanical behavior of some carbonate rocks. *Int. J. Rock Mech. Min. Sci.* **2010**, *47*, 307–312. [CrossRef]

19. Zhang, Q.B.; Zhao, J. A Review of Dynamic Experimental Techniques and Mechanical Behaviour of Rock Materials. *Rock Mech. Rock Eng.* **2014**, *47*, 1411–1478. [CrossRef]
20. Frew, D.J.; Forrestal, M.J.; Chen, W. A split Hopkinson pressure bar technique to determine compressive stress-strain data for rock materials. *Exp. Mech.* **2001**, *41*, 40–46. [CrossRef]
21. Bailly, P.; Delvare, F.; Vial, J.; Hanus, J.L.; Biessy, M.; Picart, D. Dynamic behavior of an aggregate material at simultaneous high pressure and strain rate: SHPB triaxial tests. *Int. J. Impact Eng.* **2011**, *38*, 73–84. [CrossRef]
22. Xia, K.W.; Yao, W. Dynamic rock tests using split Hopkinson (Kolsky) bar system—A review. *J. Rock Mech. Geotech. Eng.* **2015**, *7*, 27–59. [CrossRef]
23. Vecchio, K.S.; Jiang, F.C. Improved Pulse Shaping to Achieve Constant Strain Rate and Stress Equilibrium in Split-Hopkinson Pressure Bar Testing. *Metall. Mater. Trans. A* **2007**, *38*, 2655–2665. [CrossRef]
24. Frew, D.J.; Forrestal, M.J.; Chen, W. Pulse shaping techniques for testing brittle materials with a split Hopkinson pressure bar. *Exp. Mech.* **2002**, *42*, 93–106. [CrossRef]
25. Tan, L.H.; Ren, T.; Yang, X.H.; He, X.Q. A numerical simulation study on mechanical behaviour of coal with bedding planes under coupled static and dynamic load. *Int. J. Min. Sci. Technol.* **2018**, *28*, 791–797. [CrossRef]
26. Yavuz, H.; Tufekci, K.; Kayacan, R.; Cevizci, H. Predicting the dynamic compressive strength of carbonate rocks from quasi-static properties. *Exp. Mech.* **2013**, *53*, 367–376. [CrossRef]
27. Shan, R.L.; Jiang, Y.S.; Li, B.Q. Obtaining dynamic complete stress–strain curves for rock using the Split Hopkinson Pressure Bar technique. *Int. J. Rock Mech. Min. Sci.* **2000**, *37*, 983–992. [CrossRef]
28. Lei, Q.H.; Latham, J.P.; Tsang, C.F. The use of discrete fracture networks for modelling coupled geomechanical and hydrological behaviour of fractured rocks. *Comput. Geotech.* **2017**, *85*, 151–176. [CrossRef]
29. Jin, J.; Cao, P.; Chen, Y.; Pu, C.Z.; Mao, D.W.; Fan, X. Influence of single flaw on the failure process and energy mechanics of rock-like material. *Comput. Geotech.* **2017**, *86*, 150–162. [CrossRef]
30. Liu, J.; Wang, J.; Wan, W. Numerical study of crack propagation in an indented rock specimen. *Comput. Geotech.* **2018**, *96*, 1–11. [CrossRef]
31. Potyondy, D.O.; Cundall, P.A. A bonded-particle model for rock. *Int. J. Rock Mech. Min. Sci.* **2004**, *41*, 1329–1364. [CrossRef]
32. Li, X.; Zhou, Z.-L.; Ye, Z.-Y.; Ma, C.-D.; Zhao, F.-J.; Zuo, Y.-J.; Hong, L. Study of rock mechanical characteristics under coupled static and dynamic loads. *Chin. J. Rock Mech. Eng.* **2008**, *27*, 1387–1395.
33. Li, X.; Gong, F.; Zhao, J.; Gao, K.; Yin, T. Test study of impact failure of rock subjected to one-dimensional coupled static and dynamic loads. *Chin. J. Rock Mech. Eng.* **2010**, *29*, 251–260.
34. Li, X.; Gong, F.; Tao, M.; Dong, L.; Du, K.; Ma, C.; Zhou, Z.; Yin, T. Failure mechanism and coupled static-dynamic loading theory in deep hard rock mining: A review. *J. Rock Mech. Geotech. Eng.* **2017**, *9*, 767–782. [CrossRef]
35. Xie, S.; Lin, H.; Chen, Y. New constitutive model based on disturbed state concept for shear deformation of rock joints. *Arch. Civ. Mech. Eng.* **2022**, *23*, 26. [CrossRef]
36. Xie, S.; Han, Z.; Hu, H.; Lin, H. Application of a novel constitutive model to evaluate the shear deformation of discontinuity. *Eng. Geol.* **2022**, *304*, 106693. [CrossRef]
37. Xie, S.; Han, Z.; Chen, Y.; Wang, Y.; Zhao, Y.; Lin, H. Constitutive modeling of rock materials considering the void compaction characteristics. *Arch. Civ. Mech. Eng.* **2022**, *22*, 60. [CrossRef]